Periodica Polytechnica Civil Engineering

Crack-retardation Mechanism of Polymer-modified Micro-Surfacing on Bridge Deck Pavements in High-altitude Cold Regions: A 3D Thermal–mechanical Fracture Analysis

Xinyuan Liu[1], Pengjia Hui[2*], Jie Jia[3], Dekun Shi[3], Teng Zhang[3]

[1] Gansu Communication Investment Management Co., Ltd., No. 743, East Nanbinhe Road, Chengguan District, Lanzhou, 730030 Gansu Province, China
[2] Gansu Fifth Ring Road Engineering Co., Ltd., No. 118 Jianlan Road, Qilihe District, Lanzhou, 730000 Gansu Province, China
[3] School of Civil Engineering and Transportation, Northeast Forestry University, No. 26 Hexing Road, Xiangfang District, Harbin, 150040 Heilongjiang Province, China
[*] Corresponding author, e-mail: huipengjia@163.com

Received: 24 April 2026, Accepted: 07 August 2026, Published online: 14 September 2026

Abstract

Early-onset fracturing within deck layers poses a significant threat to the durability of composite steel-concrete structures, specifically those subjected to extreme multi-hazard environments characterized by extreme cold, intense solar radiation, and heavy traffic loads. This study explores the mechanism of polymer-modified micro-surfacing in inhibiting cracks on bridge decks. Utilizing the structural specifications of a representative composite girder span in northwestern China, a rigorous three-dimensional fracture mechanics model was established by integrating FRANC3D and ABAQUS. The results show that micro-surfacing acts as an excellent thermal barrier. It effectively reduces the temperature gradient within the pavement layer, thereby decreasing thermal stress accumulation at the steel-concrete interface. Furthermore, compared to conventional sealing materials, micro-surfacing has higher stiffness. It effectively disperses surface tensile stresses and significantly reduces the stress intensity at the crack tip. Therefore, micro-surfacing restricts crack opening through mechanical confinement and prevents the propagation of reflective cracks. Ultimately, this treatment significantly improves the fatigue life and structural resilience of the entire bridge system in extreme multi-hazard environments.

Keywords

steel-concrete composite bridge, high-altitude region, micro-surfacing, crack propagation, fracture mechanics, FRANC3D-ABAQUS

1 Introduction

Steel-concrete composite bridge decks are widely used in long-span infrastructure, but their pavement layers are vulnerable in high-altitude cold regions. Strong solar radiation, large diurnal temperature variation, and winter cooling generate steep temperature gradients, while repeated wheel loads concentrate stress near the steel-concrete interface [1]. Moisture, freeze-thaw action and aging can further weaken the asphalt layer and accelerate crack initiation [2, 3]. Polymer-modified micro-surfacing has been used as a preventive maintenance layer because it can improve surface sealing, skid resistance and cracking resistance [4–8]. However, most existing studies focus on material-level performance, and the coupled thermal-mechanical crack-retardation mechanism in steel-concrete composite bridge decks remains insufficiently clarified.

Fracture-mechanics-based numerical methods provide a useful route for assessing crack initiation and propagation in pavement and bridge structures [9–11]. XFEM, VCCT and continuum damage approaches have been applied to asphalt cracking and overlay tests [12–17], while bridge-deck studies have examined fatigue cracks in orthotropic steel decks using experimental and numerical methods [18–21]. These studies demonstrate that crack paths, SIFs and energy-release parameters can quantify damage evolution. Nevertheless, direct application to bridge-deck pavement treated with micro-surfacing is limited because the problem involves temperature-dependent pavement materials, interfacial stress concentration and seasonal thermal-mechanical coupling.

To overcome the limitations of mesh-dependent FEM and purely two-dimensional crack descriptions, this study adopts the FRANC3D-ABAQUS interactive framework [22, 23].

Cite this article as: Liu, X., Hui, P., Jia, J., Shi, D., Zhang, T. "Crack-retardation Mechanism of Polymer-modified Micro-Surfacing on Bridge Deck Pavements in High-altitude Cold Regions: A 3D Thermal–mechanical Fracture Analysis", Periodica Polytechnica Civil Engineering, 2026. https://doi.org/10.3311/PPci.44463

FRANC3D adaptively reconstructs the crack-front mesh during propagation, while ABAQUS provides the global thermal and mechanical response. This coupling allows mixed-mode SIFs and *J*-integral values to be evaluated along an evolving three-dimensional crack front.

A representative composite girder bridge in Lanzhou, Gansu Province, was selected as the engineering case. The study evaluates the thermal-insulation effect of micro-surfacing, simulates crack propagation under mechanical and seasonal thermal-mechanical loading, and benchmarks the simulated trends against published experimental and field-related observations. The objective is to clarify how polymer-modified micro-surfacing delays crack opening and upward propagation in bridge-deck pavement.

2 Macro-meso analysis

2.1 Methodology

2.1.1 Temperature field

Ambient temperature, solar radiation and wind speed govern the transient temperature field of asphalt pavement [24]. The bridge-deck surface exchanges heat with the environment through solar radiation, convection and long-wave radiation, while heat conduction controls the internal response. The temperature field was therefore calculated by considering solar radiation, atmospheric temperature variation and convective heat transfer.

The solar radiation $q(t)$ is given by Eq. (1) – Eq. (3) [21].

$$q(t) = \frac{0.131Q}{\pi} + \sum_{k=1}^{\infty} a_k \cos\frac{k\pi(t-12)}{12} \tag{1}$$

$$a_k = \frac{1.572Q}{\pi c}\left[\frac{1}{12/c+k}\sin\left(\frac{12}{c}+k\right)\frac{c\pi}{24} + \frac{c\pi}{24}\right], k = \frac{12}{c} \tag{2}$$

$$a_k = \frac{1.572Q}{\pi c}\left[\begin{array}{l}\frac{1}{12/c+k}\sin\left(\frac{12}{c}+k\right)\frac{c\pi}{24} + \\ \frac{1}{12/c-k}\sin\left(\frac{12}{c}-k\right)\frac{c\pi}{24}\end{array}\right], k \neq \frac{12}{c} \tag{3}$$

Where Q is the daily solar insolation, c is the effective sunshine duration, k is the harmonic order, and a_k is the Fourier coefficient of solar radiation.

The atmospheric temperature follows a regular cycle, with a warming period of approximately 10 hours and a cooling period of about 14 hours. Accordingly, the atmospheric temperature exhibits a regular diurnal variation. Consequently, the temperature variation is described by Eq. (4).

$$T = \bar{T} + T_m\left[0.96\sin\omega(t-t_0) + 0.14\sin 2\omega(t-t_0)\right]. \tag{4}$$

Where $\bar{T}$ is the average daily temperature, T_m is the daily temperature range, t_0 is the phase lag between peak solar radiation and peak air temperature, t is time, and omega is the angular frequency.

2.1.2 Fracture mechanics

Fatigue cracking in bridge-deck pavement is governed by crack-tip stress concentration and cyclic loading. The crack-growth rate can be related to the stress-intensity-factor range using Paris' law [25], as expressed in Eq. (5).

$$\frac{da}{dN} = A(\Delta K)^n \tag{5}$$

Where a is the crack length, N is the number of load cycles, da/dN is the crack growth rate, ΔK is the stress intensity factor range, and A and n are the fatigue fracture parameters of asphalt concrete.

The stress intensity factors characterize the singular stress field at the crack tip and were used to evaluate the fracture response of untreated and micro-surfacing-treated bridge-deck pavement. The three basic cracking modes are shown in Fig. 1, and the SIFs were calculated by the *M*-integral method in FRANC3D, as shown in Eq. (6) [9].

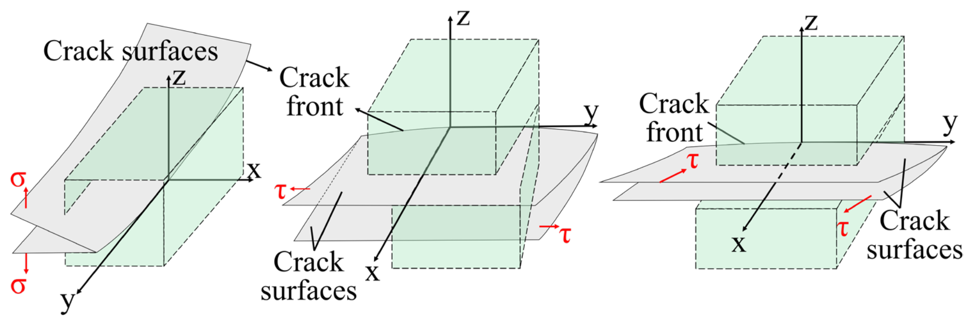

Fig. 1 Patterns of Structural Cracks: (a) Tension cracks; (b) Shear cracks; (c) Tear-off cracks

$$M = 2\left[\frac{1-v^2}{E}K_{\mathrm{I}}^{(1)}K_{\mathrm{I}}^{(2)} + \frac{1-v^2}{E}K_{\mathrm{II}}^{(1)}K_{\mathrm{II}}^{(2)} + \frac{1+v^2}{E}K_{\mathrm{III}}^{(1)}K_{\mathrm{III}}^{(2)}\right] \tag{6}$$

Where M is the interaction (M-)integral, E is Young's modulus, v is Poisson's ratio, and K_{I}, K_{II}, K_{III} are the stress intensity factors.

The J-integral was also used to quantify the crack-driving energy at the crack front, following Rice's path-independent integral formulation [26]. The J-integral values of untreated and treated specimens were calculated using Eq. (7).

$$J = \int\left(Wdy - \bar{T}\frac{\partial \bar{U}}{\partial x}ds\right) \tag{7}$$

Where W is the strain energy density, $\bar{T}$ is the external force vector exerted on the arc element ds of the integration loop, and $\bar{U}$ is the displacement vector on the integration loop.

2.2 Macro-meso modeling method

The global bridge model and local crack-propagation submodel were constructed using solid elements. C3D8 elements were used for mechanical analysis and DC3D8R elements for thermal analysis. Crack initiation was governed by the maximum principal stress criterion, and Fig. 2 shows the pavement sealing-treatment scheme.

2.3 Macro-meso analysis method

The proposed macro-meso procedure consists of material characterization, global bridge analysis, local crack-propagation simulation and feedback evaluation of pavement-seal performance. The global model provides boundary conditions for the mesoscale crack submodel, and the local fracture results are used to assess the crack-retardation effect of micro-surfacing, as shown in Fig. 3.

- Step 1: Material characterization of the steel-concrete composite girders, bridge deck pavement, and seal coats is conducted to ascertain the constituent properties for both the macroscopic and mesoscopic sub-models.

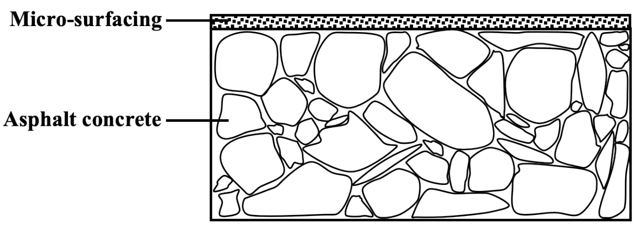

Fig. 2 Schematic diagram of micro-surfacing

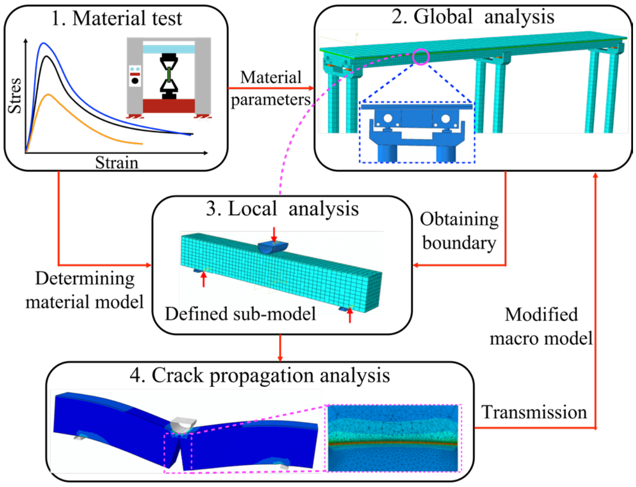

Fig. 3 Flow chart of the global-local crack propagation analysis

- Step 2: Dynamic analyses are performed on the macroscopic full-bridge model to derive dynamic boundary conditions for mesoscopic sub-models of critical regions, accounting for mechanical, thermal, and coupled loading scenarios.
- Step 3: Fracture analyses are conducted within the mesoscopic sub-model to capture crack propagation patterns in critical localized regions (vulnerable areas).
- Step 4: The crack propagation results from the mesoscale sub-model are evaluated. Subsequently, the localized fracture state is extrapolated to the macroscopic model to refine the global analysis results.
- Step 5: Guided by the crack propagation characteristics derived from the revised macroscopic model, the design parameters of the bridge deck pavement seal coat are optimized to extend the service life of the composite girder.

2.4 FRANC3D-ABAQUS interaction method

A sequential thermal-mechanical coupling strategy was adopted [27]. In the thermal analysis, the influence of the crack on heat conduction is neglected, and the transient temperature field is solved on the uncracked layered geometry, since the crack dimension is negligible relative to the overall pavement structure. The mechanical fracture model, by contrast, does not assume a measured finite pre-existing crack. Instead, a numerically seeded planar crack was introduced at the bottom of the pavement layer near the steel-concrete interface above the girder, where reflective cracking is most likely to initiate according to reported overlay and pavement-cracking observations [12, 16, 17]. The seed crack was used only to define the initial crack-front location for FRANC3D adaptive remeshing, and its dimension was treated as negligible relative to the pavement-layer thickness;

therefore, the reported SIFs and J-integral values are evaluated as functions of the subsequent propagated crack length rather than as responses to a prescribed large initial defect.

The transient temperature field was first solved on the layered bridge-deck pavement and then mapped to the mechanical fracture model as a predefined field. The initial crack was introduced near the steel-concrete interface, where reflective cracking is most likely to occur. FRANC3D adaptively remeshed the local crack-front region during propagation, while ABAQUS solved the corresponding stress field. Crack growth was evaluated using mixed-mode SIFs and J-integral values along the crack front, and the computational workflow is shown in Fig. 4.

3 Case study: steel-concrete composite bridge in a high-altitude cold region

3.1 Bridge description

The prototype bridge is a continuous steel-concrete composite girder bridge on the G312 Highway in Gansu Province, Northwest China. The bridge is located at an altitude of approximately 1700 m in a semi-arid plateau cold region with intense solar radiation, large daily temperature variation and a seasonal freeze-thaw environment.

The selected segment has a 4×40 m span arrangement and an 11.75 m wide deck. The superstructure consists of a single-cell box girder with a concrete deck slab, corrugated steel webs and steel flanges. The pavement system contains an asphalt layer above the concrete deck, with polymer-modified micro-surfacing applied as the surface treatment layer. The main geometric parameters are listed in Table 1.

3.2 Material characteristics

The thermal-mechanical properties of steel, concrete, asphalt pavement and micro-surfacing were defined according to their material roles. Steel and concrete were modeled as isotropic linear elastic materials using standard design parameters, while asphalt pavement and micro-surfacing were assigned thermal and mechanical properties based on pavement specifications and published thermal-property studies [28–32]. The adopted material parameters are summarized in Table 2.

Thermal boundary conditions included solar-radiation absorption on the top pavement surface, wind-speed-dependent convection and long-wave radiation to the sky. The lateral faces were treated as adiabatic by symmetry, and the bottom steel-girder surface exchanged heat with the surrounding air. Winter and summer meteorological inputs for Lanzhou were taken from January 12 and July 15, 2025, respectively, as listed in Tables 3 and 4.

The numerical model used a sequential coupled thermal-stress procedure in FRANC3D-ABAQUS. DC3D8R elements were used in the thermal step, and the resulting

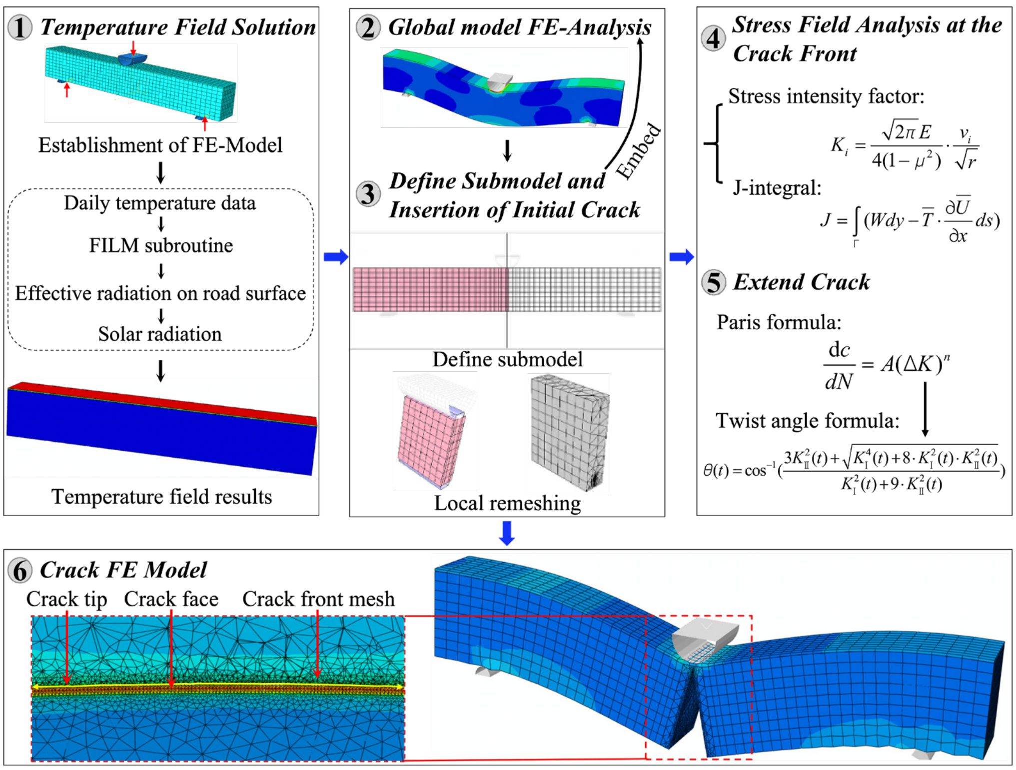

Fig. 4 Computational framework for FRANC3D-ABAQUS

Table 1 Geometric parameters

Parameter/Component	Value	Unit
Span arrangement	4×40	m
Bridge deck width	11.75	
Steel girder height	2.0	
Center-to-center spacing of girders	6.5	
Concrete slab thickness	0.28	
Micro-surfacing thickness	0.1	

Table 2 Material parameters [28–32]

Category	Parameter/Component	Value	Unit
Steel	Density	7850	kg/m³
	Elastic modulus	2.06×10^5	MPa
	Poisson's ratio	0.3	–
	Thermal expansion Coefficient	1.20×10^{-5}	°C⁻¹
	Thermal conductivity	48	W/(m×K)
	Specific heat capacity	470	J/(kg×K)
Concrete	Density	2400	kg/m³
	Elastic modulus	3.55×104	MPa
	Poisson's ratio	0.2	–
	Thermal expansion Coefficient	1.0×10^{-5}	°C⁻¹
	Thermal conductivity	1.8	W/(m×K)
	Specific heat capacity	960	J/(kg×K)
Pavement layer	Density	2450	kg/m³
	Elastic modulus	2000	MPa
	Poisson's ratio	0.25	–
	Thermal expansion Coefficient	2.4×10^{-5}	°C⁻¹
	Thermal conductivity	1.3	W/(m×K)
	Specific heat capacity	960	J/(kg×K)
	Radiation absorption	0.9	–
	Surface emission rate	0.81	–
Micro-surfacing	Density	2350	kg/m³
	Low temperature elastic Modulus	4500	MPa
	Poisson's ratio	0.3	–
	Thermal expansion Coefficient	2.0×10^{-5}	°C⁻¹
	Thermal conductivity	0.85	W/(m×K)
	Specific heat capacity	1100	J/(kg×K)
	Radiation absorption	0.9	–
	Surface emission rate	0.81	–

nodal temperatures were transferred to the mechanical model. The crack front was locally refined and propagated incrementally until the predefined crack-growth criterion was reached.

3.3 Analysis of thermal insulation mechanism

Fig. 5 shows that micro-surfacing changes the vertical heat-flux distribution in the bridge-deck pavement. In the untreated deck, heat penetrates rapidly into the pavement, whereas the treated deck shows a more diffuse heat-flux field. This indicates that polymer-modified micro-surfacing reduces direct heat transfer and functions as a thermal buffer at the pavement surface. The introduction of a high-thermal-resistance barrier reduces the peak internal heat flux by approximately 10% to 38.1% relative to the untreated reference.

The vertical temperature profiles in Fig. 6 confirm the buffering effect. In winter, the treated pavement maintains a higher internal temperature than the untreated system, reducing low-temperature brittleness and thermal contraction. In summer, micro-surfacing lowers the surface temperature and reduces the vertical gradient. Overall, the treatment decreases the temperature gradient by 10.0%-38.1%, which weakens thermally induced stress accumulation near the steel-concrete interface.

3.4 Fracture behavior under mechanical loading

Mechanical loading was first analyzed separately to establish the baseline fracture response. The reflective crack was initiated at the bottom of the pavement layer near the steel-concrete interface, consistent with reported reflective-cracking mechanisms [12, 16, 17]. Fig. 7 shows that micro-surfacing reduces both SIFs and J-integral values during upward crack growth, indicating lower crack-driving force under wheel loading.

As the crack approaches the wheel-load influence zone, the crack-tip stress field increases nonlinearly. The untreated model shows a sharper rise in fracture parameters, whereas the treated model maintains lower K_I and J-integral values. This suggests that micro-surfacing redistributes local tensile stress and restrains crack opening at the pavement surface.

3.5 Crack propagation under coupled thermal-mechanical actions

Thermal-mechanical coupling produces the most unfavorable fracture condition for the bridge-deck pavement. In winter, thermal contraction of asphalt intensifies the tensile stress generated by vehicle loading, causing higher SIFs and J-integral values in the untreated deck. As shown in Fig. 8, the treated system maintains lower fracture parameters along the crack path, demonstrating stronger resistance to unstable upward crack propagation. Under summer coupling (Fig. 9), micro-surfacing

Table 3 Meteorological parameters (Winter)

Time (h)	Temperature (°C)	Time (h)	Temperature (°C)	Time (h)	Temperature (°C)
0	−9.2	8	−13.5	16	2.5
1	−10.5	9	−11.2	17	0.8
2	−11.8	10	−8.5	18	−1.5
3	−12.9	11	−5.3	19	−3.8
4	−13.8	12	−2.1	20	−5.9
5	−14.5	13	1.2	21	−7.2
6	−15.0	14	4.2	22	−8.1
7	−14.8	15	3.8	23	−9.0
Total daily insolation (MJ/m^2)	13.8				

Table 4 Meteorological parameters (Summer)

Time (h)	Temperature (°C)	Time (h)	Temperature (°C)	Time (h)	Temperature (°C)
0	26.2	8	27.8	16	38.0
1	25.8	9	30.2	17	37.5
2	25.5	10	32.5	18	36.2
3	25.1	11	34.1	19	34.8
4	24.7	12	35.3	20	32.9
5	24.3	13	36.5	21	30.7
6	24.0	14	37.2	22	28.5
7	25.5	15	37.8	23	27.1
Total daily insolation (MJ/m^2)	25.2				

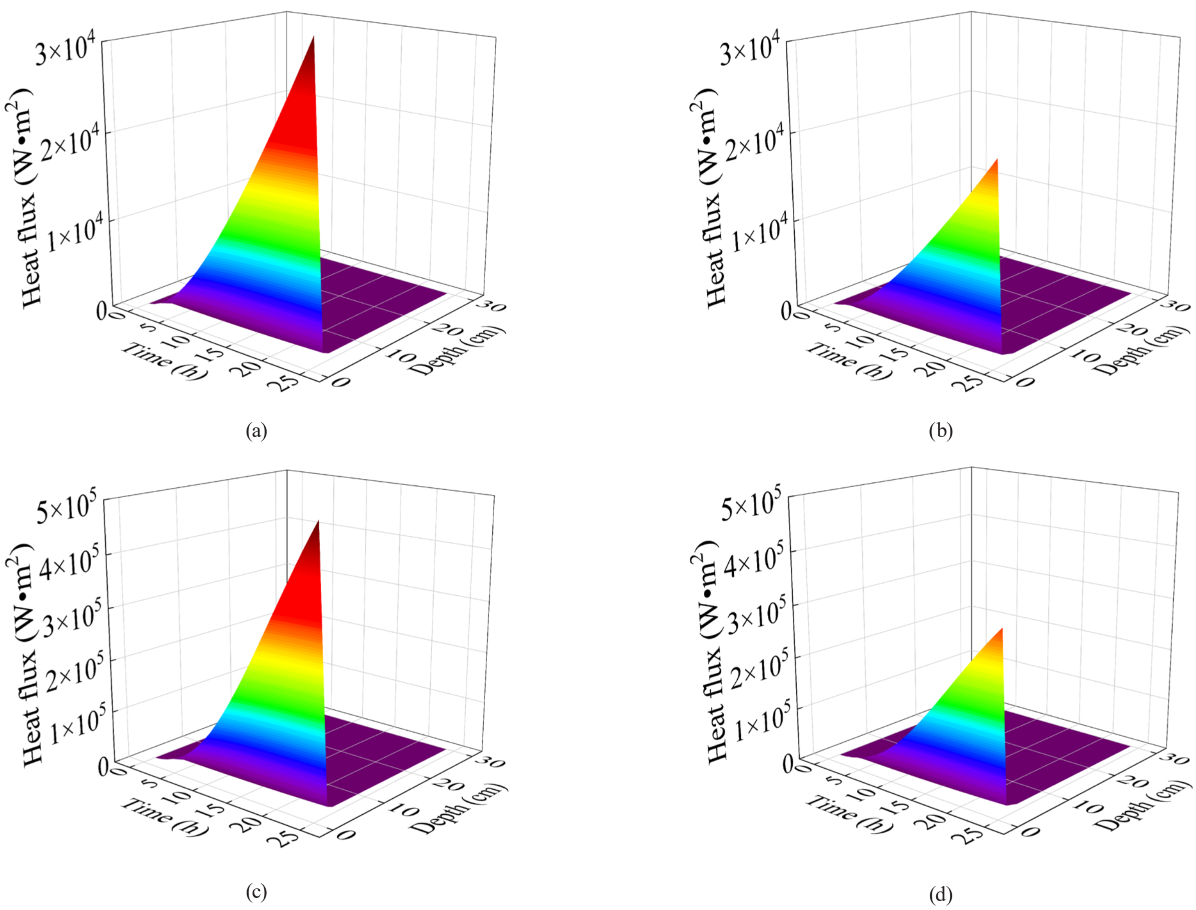

Fig. 5 Evolution of internal heat flux along the pavement depth: (a) untreated control, winter; (b) treated control, winter; (c) untreated control, summer; (d) treated control, summer

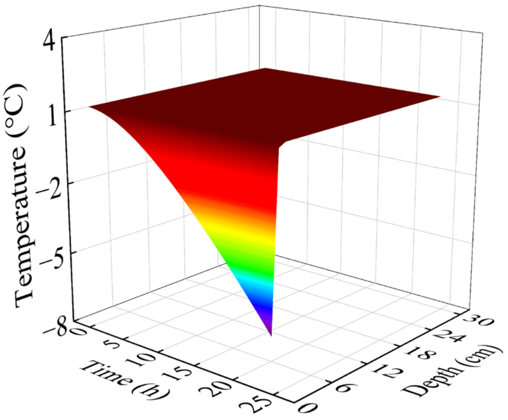

(a)

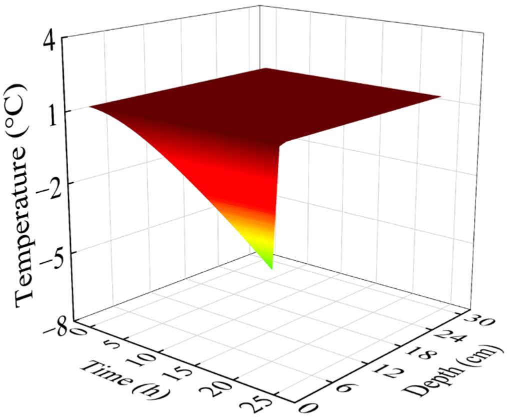

(b)

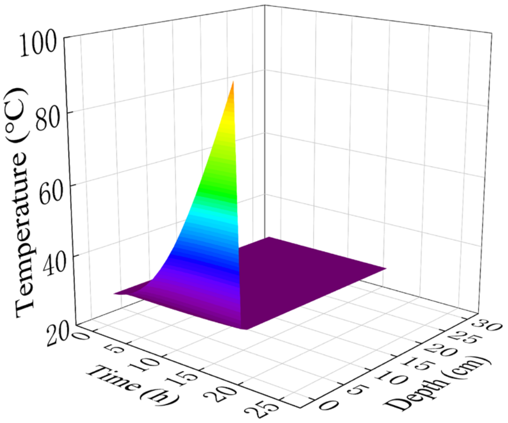

(c)

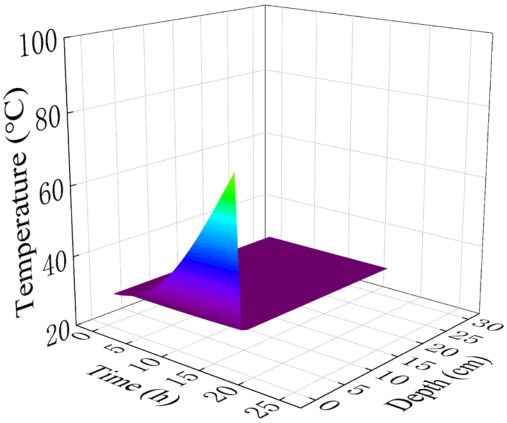

(d)

Fig. 6 Vertical temperature profiles: (a) untreated control, winter; (b) treated control, winter; (c) untreated control, summer; (d) treated control, summer.

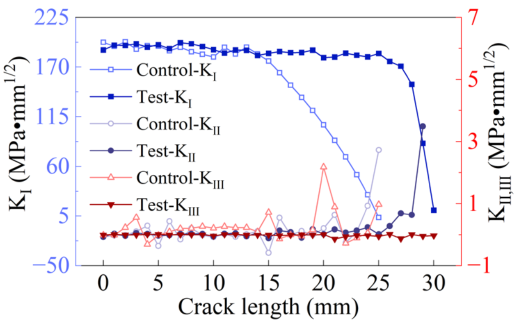

(a)

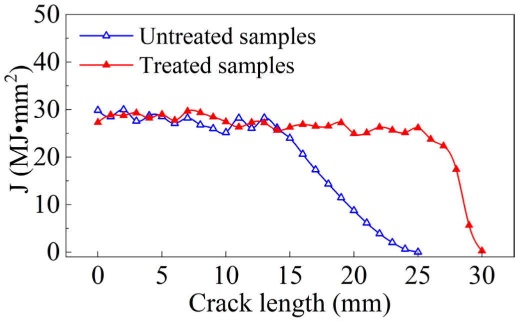

(b)

Fig. 7 Fracture parameters under Load: (a) *K*-value; (b) *J*-integral

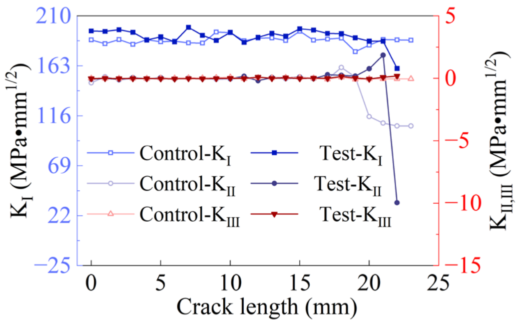

(a)

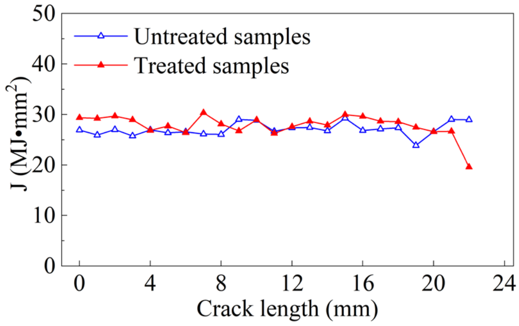

(b)

Fig. 8 Comparative evolution of fracture parameters (Winter): (a) *K*-value; (b) *J*-integral

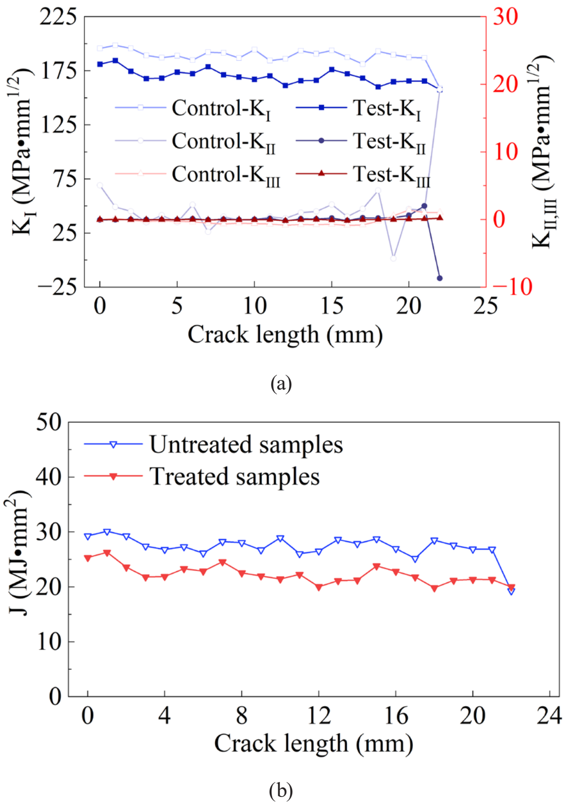

Fig. 9 Comparative Evolution of Fracture Parameters (Summer): (a) *K*-value; (b) *J*-integral

also reduces the fracture-driving parameters, although the effect is less severe than in winter.

The crack-retardation mechanism is attributed to both thermal buffering and mechanical constraint. Thermally, micro-surfacing moderates internal temperature fluctuations and reduces shrinkage-induced tensile stress. Mechanically, its surface stiffness restricts crack opening and redistributes the local crack-tip stress field. These coupled effects explain the lower SIFs and *J*-integral values observed in the treated pavement system.

3.6 Benchmarking against experimental and field observations

To address the need for comparison with experimental and field evidence, the simulated crack-propagation trends were benchmarked against published observations, as shown in Table 5. The comparison focuses on crack path, low-temperature cracking tendency, surface-treatment crack retardation and fracture-mechanics indicators.

As shown in Table 5, the simulated trends are consistent with mechanisms reported in previous experimental and field-related studies. The upward propagation from a lower high-stress interface agrees with overlay-test and DIC observations of cracking from notches or

Table 5 Benchmark comparison with published observations

Aspect	Present result	Published observation
Crack path	Upward propagation from the lower steel-concrete interface.	Overlay/DIC tests report upward cracking from notches or high-stress zones [12, 17].
Low-temperature effect	Winter coupling increases the crack-driving force.	Cold conditions increase asphalt brittleness and cracking susceptibility [16, 32].
Overlay retardation	Micro-surfacing reduces SIFs and *J*-integral values.	Modified/reinforced overlays delay cracking or reduce crack opening [4, 8, 17].
Fracture indicators	Mixed-mode SIFs and *J*-integral quantify crack evolution.	Bridge-deck studies use crack paths and fracture parameters for crack assessment [18, 21, 26].

strain-concentrated regions [12, 17]. The winter increase in crack-driving parameters is consistent with the enhanced brittleness and cracking susceptibility of asphalt at low temperature [16, 32]. The reduction in SIFs and *J*-integral values after applying micro-surfacing also agrees with observations that modified or reinforced overlays can delay crack growth and reduce crack opening [4, 8, 17]. Thus, micro-surfacing acts as both a thermal buffer and a mechanical constraint layer. This benchmark-based comparison therefore provides mechanism-level support for the simulated crack-retardation process.

4 Conclusions

This study examined the crack-retardation mechanism of polymer-modified micro-surfacing in steel-concrete composite bridge deck pavements in high-altitude cold regions using a 3D thermal-mechanical fracture framework and project-based structural parameters. The main conclusions are as follows.

Micro-surfacing acts as a thermal buffer layer. Compared with untreated decks, it reduces the vertical temperature gradient by 10.0% to 38.1%, thereby alleviating thermal stress concentration near the steel-concrete interface and lowering the tendency for interfacial cracking under severe diurnal and seasonal temperature variations.

Under wheel loading and thermal-mechanical coupling, micro-surfacing reduces the stress intensity factors (SIFs) and *J*-integral values at the crack front. This indicates a lower crack-driving force and delayed upward propagation of reflective cracks. Mechanistically, the treated layer constrains crack opening and redistributes tensile stress around the crack tip.

The benchmark comparison with published experimental and field-related observations supports the physical consistency of the simulated mechanisms, including upward crack propagation from high-stress zones, low-temperature amplification and overlay-induced crack retardation. This indicates that the simulated crack-retardation mechanism is consistent with reported experimental and field-related evidence.

The model uses idealized crack geometry, material parameters, interface conditions and selected traffic-temperature loading scenarios; future work should combine project-specific laboratory tests, field monitoring and calibrated long-term simulations to further validate the proposed mechanism.

References

[1] Wang, Z., Chen, A., Sun, J. "Analytical model on transient temperature field of reinforced concrete panels subjected to fire considering attenuation of thermal conductivity", Materials and Structures, 59(3), 148, 2026. https://doi.org/10.1617/s11527-026-03037-0

[2] Guo, M., Yin, X., Du, X., Tan Y. "Effect of aging, testing temperature and relative humidity on adhesion between asphalt binder and mineral aggregate", Construction and Building Materials, 363, 129775, 2023. https://doi.org/10.1016/j.conbuildmat.2022.129775

[3] Tian, W., Chen, Y., Pang, J. , Yang, Y., Tao, J., Tebaldi, G. "Effects of desulfurization degree on crumb rubber pretreated with heavy bio-oil on asphalt binder cracking performance at intermediate temperatures", Materials and Structures, 59(3), 140, 2026. https://doi.org/10.1617/s11527-026-03040-5

[4] Esfahani, M. A., Khatayi, A. "Effect of type and quantity of emulsifier in bitumen polymer emulsion on microsurfacing performance", International Journal of Pavement Engineering, 23(4), pp. 957–971, 2022. https://doi.org/10.1080/10298436.2020.1784416

[5] Ma, T., Wang, N., Han, C., Wang, S., Tong, Z. "Asphalt Pavement Residual Life Assessment Based on SmartRock Sensors", IEEE Transactions on Instrumentation and Measurement, 72, pp. 1–12, 2023. https://doi.org/10.1109/TIM.2023.3267372

[6] Yousuf, Z., Hlavička, V. "Sustainable Use of Construction Waste: Fire Resistance and Strength Characteristics of Recycled Aggregate Concrete for Sustainable Concrete", Periodica Polytechnica Civil Engineering, 69(4), pp. 1216–1228, 2025. https://doi.org/10.3311/PPci.40330

[7] Bhargava, N., Siddagangaiah, A. K., Ryntathiang, T. L. "Systematic approach to address challenges in microsurfacing mix design", Construction and Building Materials, 270, 121759, 2021. https://doi.org/10.1016/j.conbuildmat.2020.121759

[8] Hu, C., Zhao, J., Leng, Z., Partl, M. N., Li, R. "Laboratory evaluation of waterborne epoxy bitumen emulsion for pavement preventative maintenance application", Construction and Building Materials, 197, pp. 220–227, 2019. https://doi.org/10.1016/j.conbuildmat.2018.11.223

[9] Yau, J. F., Wang, S. S., Corten, H. T. "A Mixed-Mode Crack Analysis of Isotropic Solids Using Conservation Laws of Elasticity", Journal of Applied Mechanics, 47(2), pp. 335–341, 1980. https://doi.org/10.1115/1.3153665

[10] Németh, G., Kovács, N. "Investigation of the Failure Modes of Embedded Corrugated Shear Connections in Steel-concrete Composite Girders", Periodica Polytechnica Civil Engineering, 70(2), pp. 424–435, 2026. https://doi.org/10.3311/PPci.41637

[11] Qing, L., Zhang, Y., Hu, Y., Yu, K. "Study on the different roles of steel and PVA fibers in the fracture evolution of hybrid fiber reinforced cementitious composites", Materials and Structures, 59(2), 109, 2026. https://doi.org/10.1617/s11527-026-03000-z

[12] Alrashydah, E., Papagiannakis, A. T. "Asphalt concrete crack propagation parameters from XFEM modelling of the Texas Overlay Test", International Journal of Pavement Engineering, 24(2), 2111564, 2023. https://doi.org/10.1080/10298436.2022.2111564

[13] Zhang, B., Yu, J., Chen, W., Liu, H. "Failure evolution and fiber toughing mechanism of ultra-high performance concrete under uniaxial compression", Journal of Sustainable Cement-Based Materials, 12(4), pp. 441–459, 2023. https://doi.org/10.1080/21650373.2022.2076264

[14] Jin, G. L., Zhang, Z. X., Huang, X. M. "Fatigue Cracking Analysis of Asphalt Concrete Based on Coupled XFEM-Continuum Damage Mechanics Method", Journal of Materials in Civil Engineering, 33(1), 04020425, 2021. https://doi.org/10.1061/(ASCE)MT.1943-5533.0003503

[15] Li, H., Luo, X., Gu, Z., Chen, Q., Zhang, Y. "Predicting crack growth of paving materials under indirect tensile fatigue loads", International Journal of Fatigue, 175, 107818, 2023. https://doi.org/10.1016/j.ijfatigue.2023.107818

[16] Du, J. H., Li, F. "Propagation Characteristics of Dispersion Cracks in Asphalt Concrete at Low Temperatures", Journal of Materials in Civil Engineering, 36(7), 04024179, 2024. https://doi.org/10.1061/JMCEE7.MTENG-17352

[17] Sudarsanan, N., Zeng, Z. A., Kim, Y. R. "Laboratory investigation into the crack propagation mechanism of geosynthetic reinforced asphalt concrete using digital image correlation technique", International Journal of Pavement Engineering, 24(1), 2251079, 2023. https://doi.org/10.1080/10298436.2023.2251079

[18] Xiang, C., Wang, D., Wang, B., Chen, A., Ma, R. "Numerical simulation of root-deck crack propagation of orthotropic steel bridge deck", Structure and Infrastructure Engineering, 18(7), pp. 1076–1090, 2022. https://doi.org/10.1080/15732479.2022.2039219

[19] Lu, N., Liu, J., Wang, H., Yuan, H.kulc, Luo, Y. "Stochastic Propagation of Fatigue Cracks in Welded Joints of Steel Bridge Decks under Simulated Traffic Loading", Sensors, 23(11), 5067, 2023. https://doi.org/10.3390/s23115067

[20] Zeng, Y., Wang, S., Xue, X., Tan, H., Zhou, J. "Fatigue Life Evaluation of Orthotropic Steel Deck of Steel Bridges Using Experimental and Numerical Methods", Sustainability, 15(7), 5945, 2023. https://doi.org/10.3390/su15075945

[21] Wang, Z., He, J., Lu, N., Liu, Y., Yin, X., Xin, H. "Experimental and numerical investigation on penetrating cracks growth of rib-to-deck welded connections in orthotropic steel bridge decks", Structures, 61, 106058, 2024. https://doi.org/10.1016/j.istruc.2024.106058

[22] Dassault Systemes "Abaqus, (2022)", [computer program] Available at: https://www.3ds.com/products/simulia/abaqus [Accessed: 22 April 2026]

[23] Fracture Analysis Consultants "FRANC3D: FRacture ANalysis Code for 3D (8.5.2)", [computer program] Available at: https://www.franc3d.com [Accessed: 22 April 2026]

[24] Assogba, O. C., Tan, Y., Zhou, X., Zhang, C., Anato, J. N. "Numerical investigation of the mechanical response of semi-rigid base asphalt pavement under traffic load and nonlinear temperature gradient effect", Construction and Building Materials, 235, 117406, 2020. https://doi.org/10.1016/j.conbuildmat.2019.117406

[25] Liu, Z., Guo, T., Chai, S. "Probabilistic Fatigue Life Prediction of Bridge Cables Based on Multiscaling and Mesoscopic Fracture Mechanics", Applied Sciences, 6(4), 99, 2016. https://doi.org/10.3390/app6040099

[26] Rice, J. R. "A Path Independent Integral and the Approximate Analysis of Strain Concentration by Notches and Cracks", Journal of Applied Mechanics, 35(2), pp. 379–386, 1968. https://doi.org/10.1115/1.3601206

[27] Fu, H., Liang, X., Chen, K., Wang, Y., Xiao, Z. "Study on key mechanical properties of the flexible spoke non-pneumatic tire considering thermo-mechanical coupling", Advances in Engineering Software, 173, 103281, 2022. https://doi.org/10.1016/j.advengsoft.2022.103281

[28] Ministry of Housing and Urban-Rural Development of the People's Republic of China "GB 50017-2017 钢结构设计标准" (Standard for design of steel structures), Beijing, China, 2017. (in chinese)

[29] Ministry of Housing and Urban-Rural Development of the People's Republic of China "GB 50010-2010 混凝土结构设计规范" (Code for Design of Concrete Structures), Beijing, China, 2010. (in chinese)

[30] Ministry of Transport of the People's Republic of China "JTG D50-2017 公路沥青路面设计规范" (Specifications for Design of Highway Asphalt Pavement), China, Beijing, 2017. (in chinese)

[31] Liu, Y., Qian, Z., Hu, H. "Thermal field characteristic analysis of steel bridge deck during high-temperature asphalt pavement paving", KSCE Journal of Civil Engineering, 20(7), pp. 2811–2821, 2016. https://doi.org/10.1007/s12205-016-0027-2

[32] Islam, M. R., Tarefder, R. A. "Coefficients of Thermal Contraction and Expansion of Asphalt Concrete in the Laboratory", Journal of Materials in Civil Engineering, 27(11), 04015020, 2015. https://doi.org/10.1061/(ASCE)MT.1943-5533.0001277